# Seasonal variability of the fatty acid composition in Aurelia aurita (Cnidaria: Scyphozoa)

Stenvers, Vanessa; Chi, Xupeng; Javidpour, Jamileh

*Published in:*
Journal of Plankton Research

*DOI:*
10.1093/plankt/fbaa026



*Publication date:*
2020

Journal of Alloys and Compounds 836 (2020) 155448

Contents lists available at ScienceDirect

Journal of Alloys and Compounds

journal homepage: http://www.elsevier.com/locate/jalcom

# Tailoring vapor-deposited ZnMg–Zn bilayer coating for steels by diffusion-driven phase transformation

S. Sabooni [a], E. Galinmoghaddam [a], A.A. Turkin [b], L.Q. Lu [a], R.J. Westerwaal [c], C. Boelsma [c], E. Zoestbergen [c], Y.T. Pei [a, *]

[a] Department of Advanced Production Engineering, Engineering and Technology Institute Groningen, University of Groningen, Nijenborgh 4, 9747 AG, Groningen, the Netherlands
[b] National Science Center "Kharkiv Institute of Physics and Technology", Akademichna St. 1, 61108, Kharkiv, Ukraine
[c] Tata Steel Nederland Technology B.V., P.O. Box 1000, 1970 CA, IJmuiden, the Netherlands

ARTICLE INFO

*Article history:*
Received 13 December 2019
Received in revised form
4 April 2020
Accepted 29 April 2020
Available online 4 May 2020

*Keywords:*
ZnMg-Zn bilayer Coatings
Adhesion
Diffusion-limited growth model
Phase transformation
Corrosion
Physical vapor deposition (PVD)

ABSTRACT

This study reports a "high temperature fast annealing" approach to tailor the microstructure of ZnMg–Zn bilayer coatings through a diffusion-driven phase transformation and to improve the adhesion strength and corrosion resistance, simultaneously. Selection of the appropriate annealing condition, 250 °C for 3 min, promotes the formation of $MgZn_2$ on the topmost surface of the coating and $Mg_2Zn_{11}$ at the interface of ZnMg/Zn. This results to an increase of the adhesion strength from 65 MPa in the as-deposited condition to 82 MPa after annealing as well as a reduction in the corrosion current density from 0.91 to 0.52 μA/cm$^2$, indicating enhanced corrosion resistance. The diffusion of the elements at high temperatures is also modeled to predict the stability region of phases during the annealing treatment. An excellent correlation is obtained between simulation and the experimental results.


## 1. Introduction

Zinc is a well-known protective coating for steels as it acts as a barrier layer and sacrificial anode against environmental corrosion [1]. In the past decades, many efforts have been made to improve the corrosion resistance of zinc coated steels by the addition of alloying elements. These efforts finally led to the alloying with Mg and/or Al [2–5] which is feasible in an industrial scale. The addition of such elements to the pure Zn coatings promotes the formation of a dense corrosion product, "Simonkolleite", acting as a barrier to corrosive environment [6]. Despite the advantage of Mg for the corrosion resistance, it reduces the adhesion of the coating to the steel substrate which is not favorable for practical applications [7].

Different strategies can be utilized to improve the adhesion of ZnMg coatings to steels substrate. It includes the addition of a more ductile interlayer [7] and the modification of chemical composition [7]. Annealing treatment can also be considered as a potential solution to improve the adhesion strength through the diffusion of elements across the interface [8]. It was reported that heat treatment enhanced the adhesion strength of thermal barrier coatings, which was attributed to the effect of diffusion on the bonding mechanism at the interface of particles [8]. The reduction of internal stress by heat treatment was also mentioned as another reason for the adhesion improvement. However, previous researches on the ZnMg coatings [9,10] did not report any positive effect of the annealing treatment on the adhesion behavior. It was claimed that the bi-layered or multi-layered ZnMg coatings lost their adhesion after a heat treatment process. Different explanations were put forward on the possible causes for the loss of adhesion of ZnMg coatings during annealing, such as the formation of brittle intermetallic compounds on the top layer [9] and the diffusion of Mg toward the steel/Zn interface [10]. It has been observed that during annealing of the as-deposited ZnMg–Zn coatings, the thickness of the Zn interlayer ($t_{Zn}$) reduces and the thickness of the ZnMg top layer ($t_{ZnMg}$) increases gradually due to the diffusion of elements across the interface [11]. It has been found out that the annealing at 180 °C can slightly improve the interfacial adhesion strength of the ZnMg–Zn bilayer coating. However, the reduction of $t_{Zn}$ to less than a threshold value may deteriorate the

* Corresponding author.
*E-mail address:* y.pei@rug.nl (Y.T. Pei).

https://doi.org/10.1016/j.jallcom.2020.155448

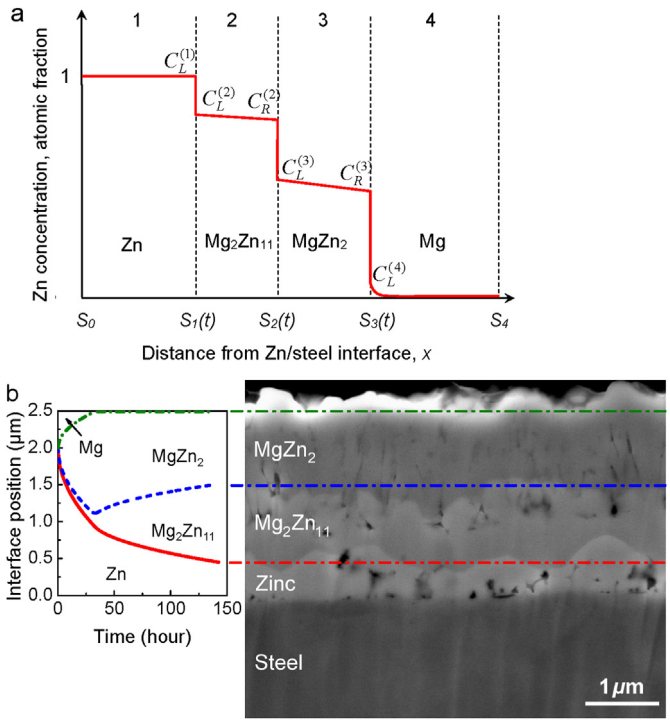


**Fig. 1.** (a) Schematic presentation of the concentration profile of Zn in the multiphase system with moving interfaces $S_n$, $n = 1, 2, 3$. The positions of the left and right boundaries ($S_{0,4}$) are fixed. (b) The stability region of phases during the annealing of a pure Zn–Mg bilayer coating at 180 °C along with the corresponding SEM micrograph.

adhesion performance of the bilayer coatings during the bending test [11]. In the present investigation, the diffusion of the elements across the ZnMg/Zn interface is modeled to predict the possible phase transformations and the stability region of phases during the annealing at high temperatures. The effect of "high temperature fast annealing" is also studied on the adhesion strength and the corrosion resistance of ZnMg–Zn bilayer coating with the aim of improving the coating properties.

## 2. Materials and methods

Thermal vapor deposition technique was used to deposit a ZnMg–Zn bilayer coating containing 11 wt% Mg on a low carbon steel substrate. This was done through evaporation and desublimation of pure Zn and ZnMg alloy on a running steel strip. Prior to the deposition, the surface of the steel substrate was cleaned by magnetron sputtering with $Ar^+$ ions. Details of the physical vapor deposition (PVD) setup and the deposition procedure can be found elsewhere [4,7]. Fast annealing treatment of the as-deposited ZnMg–Zn bilayer coating was performed using a ceramic heater with an ultrafast ramp rate up to 150 °C/s. As the diffusion rate of elements at 180 °C is too slow [11], 250 and 280 °C were selected as the annealing temperatures. The duration of the annealing was considered up to 180 min.

The microstructure of the as-deposited and annealed samples was investigated by scanning electron microscopy (SEM, Philips XL30-ESEM), scanning transmission electron microscopy (STEM, FEI Helios G4) and transmission electron microscopy (TEM, JEOL 2010F). CSM Revetest scratch tester was employed to evaluate the "adhesion strength" of the coatings at the ZnMg/Zn interface using the modified Benjamin-Weaver model recently developed [7,11]. The scratch tests were performed using a Rockwell C diamond indenter with a continuously increasing normal load from 0.5 N to 20 N. The loading rate was considered as 20 N/min for all experiments. The critical load of delamination ($L_c$) was defined as the normal load at which a continuous delamination was observed at the interface during the scratch test. The "adhesion performance" of the coatings under bending was also qualified by the BMW crash adhesion test, commonly used in industry to evaluate the adhesion performance of galvanized coatings [10]. Clear distinction should be made between the two terms "adhesion strength" and "adhesion performance". The former is an intrinsic property of the interface and can be well measured by scratch test, and the latter is more extrinsic depending on the actual loading condition.

Potentiodynamic polarization tests were performed to evaluate the corrosion behavior of the samples. The tests were carried out in a 3.5 wt% NaCl solution at room temperature, and the Pt foil electrode was used as the counter electrode. Prior to each test, the samples (working electrodes) were kept in the solution for 10 min to reach the open circuit potential. To minimize the ohmic potential drop, the reference electrode (silver chloride electrode, potential 0.210 V at 25 °C with respect to standard hydrogen electrode) was placed close to the working electrode (ZnMg–Zn coated steel). The Tafel polarization curves were obtained at a constant scan rate of 0.5 mV/s, starting from a potential of −1.4 V to −0.8 V vs. SCE. As the surface roughness of the galvanized coatings influences the anodic dissolution process [12], the roughness of the coatings was also measured by atomic force microscopy (AFM, Dimension 3100).

## 3. Results and discussion

### 3.1. Diffusion-limited growth of the intermetallic phases in ZnMg–Zn bilayer coatings

In this section, a phenomenological model is formulated which describes the diffusion-limited growth of intermetallic phases in the bilayer coatings during annealing. The model starts with the diffusion couple consisting of pure Mg and Zn layers (0.7 μm thick Mg on top of 2 μm thick Zn) on steel. By annealing, $MgZn_2$ and $Mg_2Zn_{11}$ intermetallic compounds form due to the reaction of pure Mg and pure Zn. As discussed later in section 3.2, after a short time annealing (e.g. 3 min at 250 °C) a very thin layer of Fe–Zn intermetallic compound (~ 50 nm thick) is observed at the interface of steel and Zn layer and remains until the full dissolution of Zn layer into the transformed ZnMg. These observations indicate that the rate of phase transformation at the interface between the steel substrate and the intermediate Zn layer is slow compared to the interdiffusion in the Zn–Mg system [11]. For this reason, in the following it is assumed that the interface between the steel substrate and the Zn layer is fixed. The composition profile across the

**Table 1**
Characteristics of the as-deposited and annealed ZnMg11–Zn bilayer coating on the steel substrate.

| Coating | $t_{Zn}$ (μm) | $t_{ZnMg}$ (μm) | Mg content (wt.%) | Roughness, $R_a$ (nm) |
|---|---|---|---|---|
| As-deposited | 1.7 | 2.3 | 11 | 52.0 |
| Annealed at 250 °C–3 min | 1.1 | 2.8 | 8 | 53.2 |
| Annealed at 280 °C–3 min | 0.9 | 3.0 | 6.5 | 53.6 |
| Annealed at 280 °C–10 min | 0.5 | 3.5 | 6 | 81.8 |

Zn–Mg system is shown schematically in Fig. 1a.

Following Darken approach, the diffusion in this binary system is described by Zn concentration $C_n(x,t)$ and the concentration-dependent interdiffusion coefficient $D_n(C_n)$

$$\frac{\partial C_n(x,t)}{\partial t} = \frac{\partial}{\partial x}\left(D_n \frac{\partial C_n(x,t)}{\partial x}\right),\ n = 1,\ldots,4 \tag{1}$$

where $n$ enumerates the phase layers. The positions of the moving phase boundaries are given by

$$\frac{dS_n(t)}{dt} = \frac{1}{C_L^{n+1} - C_R^n}\left(D_n \frac{\partial C_n}{\partial x}\bigg|_{x=S_n(t)} - D_{n+1}\frac{\partial C_{n+1}}{\partial x}\bigg|_{x=S_n(t)}\right),\ n = 1,2,3 \tag{2}$$

For the sake of simplicity Eqs. (1) and (2) ignore the variation in atomic volumes of Zn and Mg in the intermetallic phases. In the diffusion-controlled moving boundary problem, the concentrations of phases in contact with each other are generally fixed by a requirement of local thermodynamic equilibrium at the interfaces [13]. In this case, concentrations at the interfaces equal to the thermodynamic equilibrium values $C_{L,R}^n$ as shown in Fig. 1a:

$$C_n|_{x=S_{n-1}(t)} = C_L^n,\ n = 2,3,4 \tag{3}$$

$$C_n|_{x=S_n(t)} = C_R^n,\ n = 1,2,3 \tag{4}$$

The maximum solubility of Mg in Zn is reported as 0.3 at.% at 400 °C [14]. The solubility of Zn in Mg is higher and is calculated as 2.5 at.% at 340 °C [15]. Diffusion of Zn from the left to the right side of Fig. 1a is maintained by the concentration gradients in the intermetallic layers. Therefore, one has to admit that $C_L^n > C_R^n$. The difference between $C_L^n$ and $C_R^n$ is the solubility range of the phase in the $n^{th}$ layer. The solubility range of the intermediate solid solution ($MgZn_2$) was determined as 1, 1.3, and 2.1 at.% at 250, 275, and 300 °C, respectively [16]. Using these data, the temperature dependence of the solubility range is approximated by the Arrhenius equation:

$$\Delta C^{(3)} = C_L^{(3)} - C_R^{(3)} = 1490 \times \exp(-0.544eV / k_B T), \tag{5}$$

where $C_R^{(3)} = 2/3$ is the atomic fraction of Zn in $MgZn_2$.

In contrast to the intermediate solid solution $MgZn_2$, the intermetallic phase $Mg_2Zn_{11}$ is a stoichiometric compound. Therefore, the solubility (homogeneity) range $\Delta C^{(2)} = C_L^{(2)} - C_R^{(2)}$ of $Mg_2Zn_{11}$ is assumed to be smaller than that of the $MgZn_2$ and is treated as a fitting parameter in the calculations.

At the external boundaries, the zero flux conditions are imposed:

$$\frac{\partial C_1}{\partial x}\bigg|_{x=S_0} = 0,\ \frac{\partial C_4}{\partial x}\bigg|_{x=S_4} = 0 \tag{6}$$

The nucleation stage is not considered here. Instead, two thin layers of intermetallic phases are inserted between the pure Zn and Mg layers as an initial condition to simulate the diffusion-limited growth of intermetallic phases. The initial distribution of Zn is simple, i.e. constant concentrations in the corresponding layers:

$$C_1|_{t=0} = 1,\ C_2|_{t=0} = 11/13,\ C_3|_{t=0} = 2/3,\ C_4|_{t=0} = 0 \tag{7}$$

The initial position of the interfaces was considered according to the initial thickness of the layers, $t_i$:

$$S_n(0) = \sum_{i=1}^{n} t_i(0) \tag{8}$$

The testing of our model with reasonable values of diffusion coefficients and interface concentrations for pure Zn and Mg layers (layers 1 and 4) has shown that these parameters do not essentially influence the growth of intermetallic layers in the Zn–Mg system. The reason is low mutual solubility of Zn and Mg at moderate

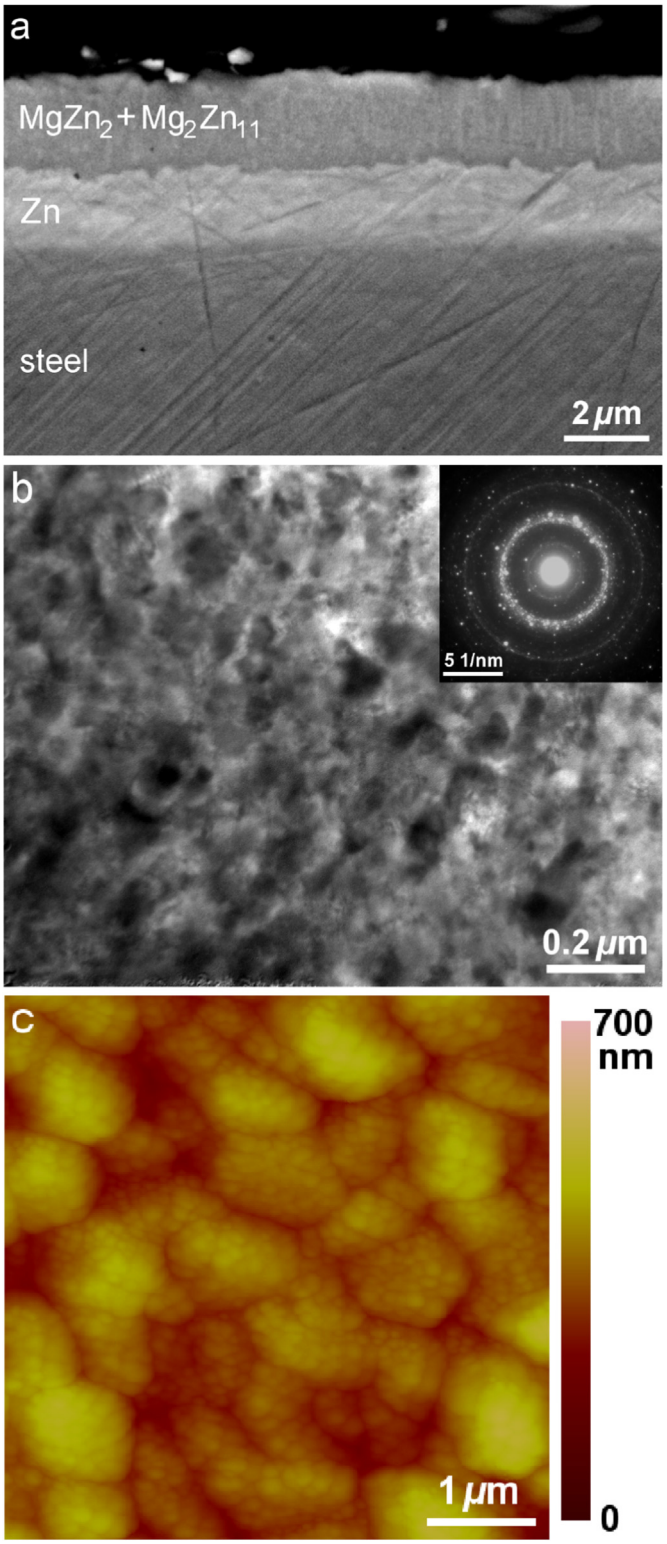


**Fig. 2.** (a) SEM micrograph showing the cross section of the as-deposited ZnMg11–Zn coating, (b) TEM micrograph of the ZnMg top layer and (c) surface morphology of the as-deposited ZnMg11–Zn coating.

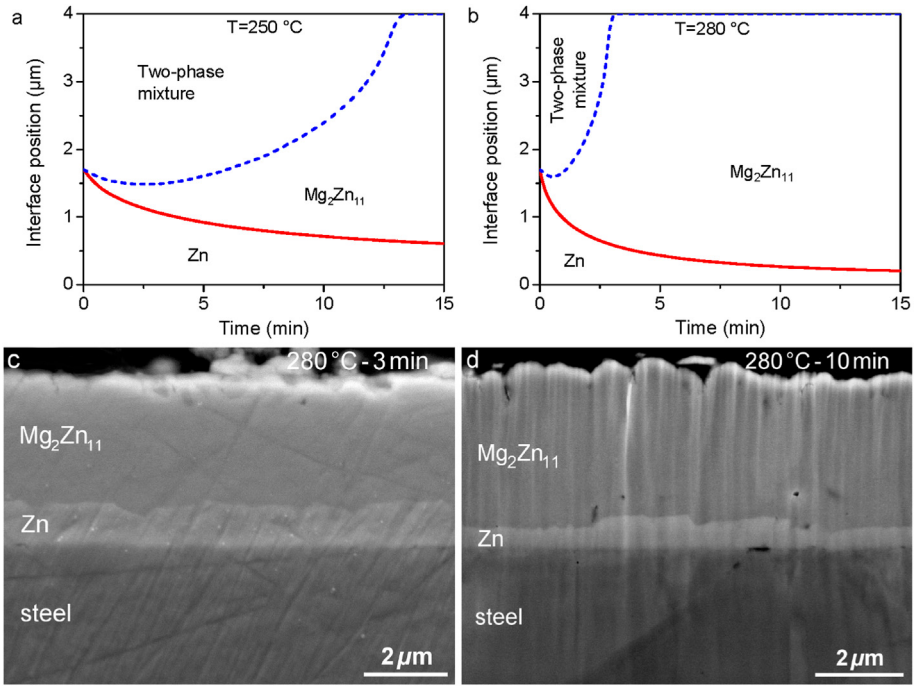


**Fig. 3.** The stability region of phases modeled for the annealing of a ZnMg11–Zn coating at 250 °C (a) and 280 °C (b). Cross sectional SEM micrograph of the annealed sample at 280 °C for 3 min (c) and 10 min (d).

temperatures, i.e. $\Delta C^{(1)} = C_L^{(1)} - C_R^{(1)} < 2.5 \times 10^{-3}$ and $\Delta C^{(4)} = C_L^{(4)} - C_R^{(4)} < 2.5 \times 10^{-2}$ [15,16]. The most important parameters which influence the growth of intermetallic layers in the Zn–Mg system are solubility ranges of $Mg_2Zn_{11}$ and $MgZn_2$ and corresponding interdiffusion coefficients in these phases.

Fig. 1b shows the stability region of the phases during annealing of a diffusion couple of a pure Zn–Mg coating ($t_{Zn} = 2$ μm, $t_{Mg} = 0.7$ μm) during annealing at 180 °C up to 150 h. It is worth to mention that the time dependence of interface positions between the layers was calculated using the experimental values of interdiffusion coefficients [17]:

$$D_{Mg_2Zn_{11}}(T) = 7.2 \times 10^{-5} \exp(-1.072/k_BT)$$
$$D_{MgZn_2}(T) = 6.62 \times 10^{-5} \exp(-0.947/k_BT) \quad (9)$$

and the solubility range of $Mg_2Zn_{11}$ intermetallic $\Delta C^{(2)} = 0.1\%$.

The thickness of the Zn layer decreases over time and the intermetallic $MgZn_2$ and $Mg_2Zn_{11}$ layers are formed due to the reaction of the elements. The Mg layer is completely consumed after sufficient annealing time (35 h in this case). The validity of the developed diffusion model can be verified by the microstructure of the 144 h annealed Zn–Mg bilayer system shown in Fig. 1b.

Assuming that the top layer of the coating is a ZnMg alloy instead of pure Mg, the model described above needs some modification considering that the initial microstructure of the top layer can be a mixture of two intermetallic compounds before annealing. In this case, the diffusion of Zn from the interlayer toward the top layer during the annealing results in the formation of a $Mg_2Zn_{11}$ layer and coarsening of the two-phases microstructure. The interface between the newly formed $Mg_2Zn_{11}$ layer and the top layer is rough. Therefore, the approximate location of the interface can be defined as a location where the concentration of Zn is less than the stoichiometric concentration in $Mg_2Zn_{11}$ by 1 at.%:

$$C(x)|_{x=S_2(t)} = 11/13 - 0.01 \quad (10)$$

The diffusion of Zn in the two-phase region is described with Eq. (1) for the mean Zn concentration:

$$C = C_{Mg_2Zn_{11}} X + C_{MgZn_2}(1 - X) \quad (11)$$

where $X$ is the volume fraction of $Mg_2Zn_{11}$. The interdiffusion coefficient in the two-phase mixture is approximated by weighted average:

$$D(C) = D_{Mg_2Zn_{11}} X + D_{MgZn_2}(1 - X) \quad (12)$$

The diffusion model formulated above is solved numerically. Using the transformation of space variable [18], the moving boundary problem is reduced to an equivalent fixed boundary problem which is solved by standard methods developed for partial differential equations.

### 3.2. Microstructure and adhesion strength

Table 1 lists the characteristics of the as-deposited and annealed ZnMg11–Zn bilayer coatings. Fig. 2 shows the cross sectional SEM, TEM and AFM micrographs of the as-deposited ZnMg11–Zn coating. The thickness of the Zn interlayer and ZnMg top layer are 1.7 μm and 2.3 μm, respectively. The microstructure of the ZnMg top layer is composed of a mixture of finely distributed nanocrystalline $Mg_2Zn_{11}$ and $MgZn_2$ intermetallic compounds (Fig. 2b) [19]. The average surface roughness ($R_a$) of the as-deposited coating was measured as 52 ± 3 nm (Fig. 2c).

To accelerate phase transformations during the annealing (considering low diffusion rate at 180 °C), the temperature was increased to 250 and 280 °C. Fig. 3a and b shows the stability region of the phases during annealing of the ZnMg–Zn coating at 250 and 280 °C, respectively, as predicted by the diffusion model. In both cases, similar behavior is observed. However, due to higher diffusion rate of elements at higher temperatures, phase transformations occur faster at 280 °C than at 250 °C. As seen, the

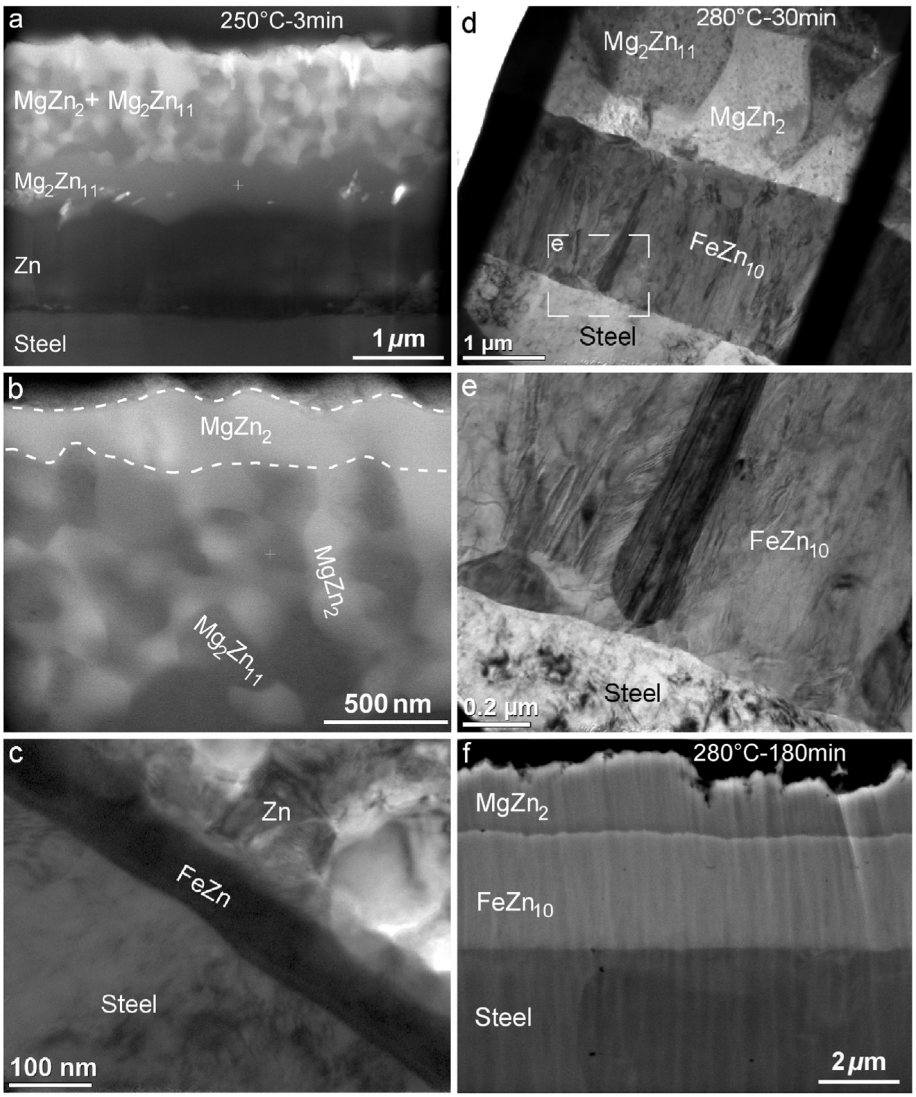


**Fig. 4.** (a–c) STEM and TEM micrographs of the annealed coating at 250 °C for 3 min. (d, e) TEM micrographs of the annealed coating at 280 °C for 30 min and (f) SEM micrograph showing the cross section of the annealed coating at 280 °C for 180 min.

thickness of the Zn interlayer decreases gradually with increasing the annealing time while the total thickness of the ZnMg top layer ($Mg_2Zn_{11}$ + the two-phase mixture) increases simultaneously. Fig. 3c and d shows the cross sectional SEM micrograph of the coating annealed at 280 °C for 3 and 10 min, respectively. The thickness of the Zn interlayer is reduced to 0.9 μm and 0.5 μm, and the thickness of the ZnMg top layer is increased to 3.0 μm and 3.5 μm, respectively, after annealing. The result of annealing treatment summarized in Table 1 verifies the model shown in Fig. 3a and b. EDS analysis reveals that the average Mg concentration of the top layer is also reduced with increasing the annealing time. The Mg concentration of the top layer after annealing of 3 and 10 min at 280 °C is lowered to 6.5 and 6 wt% Mg, respectively. This corresponds to the stoichiometric concentration of $Mg_2Zn_{11}$.

In addition to the reduction of the thickness of Zn layer during annealing, a thin layer of $Mg_2Zn_{11}$ forms on top of the Zn interlayer at the early stage of annealing and extends with further annealing until it covers the entire top layer. Fig. 4a–b shows the STEM micrographs of the annealed sample at 250 °C for 3 min. A thin layer of $Mg_2Zn_{11}$ is formed due to the upward diffusion of Zn and the resultant Mg concentration drop in this layer, which results in a 2.8 μm thick composite top layer and thinned Zn intermediate layer of 1.1 μm thick. More interesting is the formation of a thin and dense outmost surface layer of $MgZn_2$ intermetallic compound (marked by the dashed lines in Fig. 4b). EDS analysis reveals that the average Mg concentration of the ZnMg for the sample annealed at 250 °C for 3 min is ~8 wt%, which is lower than the as-deposited coating and higher than the sample annealed at 280 °C for the same duration of annealing. In addition, a very thin layer of Fe–Zn intermetallic compound (~50 nm thick) is also observed at the interface of Zn layer and steel substrate (Fig. 4c). At longer annealing times (≥20 min at 280 °C), the Zn intermediate layer is fully dissolved and instead, a thick layer of Fe–Zn intermetallic compound containing 9 wt% of Fe (δ phase) is formed at the interface of steel/ZnMg (see Fig. 4d–e). The formation and growth of the Fe–Zn intermetallic consume some of the contained Zn of the top layer. This results in the saturation of the top layer with Mg and promotes a reverse phase transformation of $Mg_2Zn_{11}$ to $MgZn_2$. Both $MgZn_2$ and $Mg_2Zn_{11}$ phases are visible in the microstructure of the 30 min annealed sample at 280 °C (Fig. 4d–e). Further growth of the $FeZn_{10}$ intermetallic is coupled with the growth of $MgZn_2$ until it fully covers the top layer (Fig. 4f).

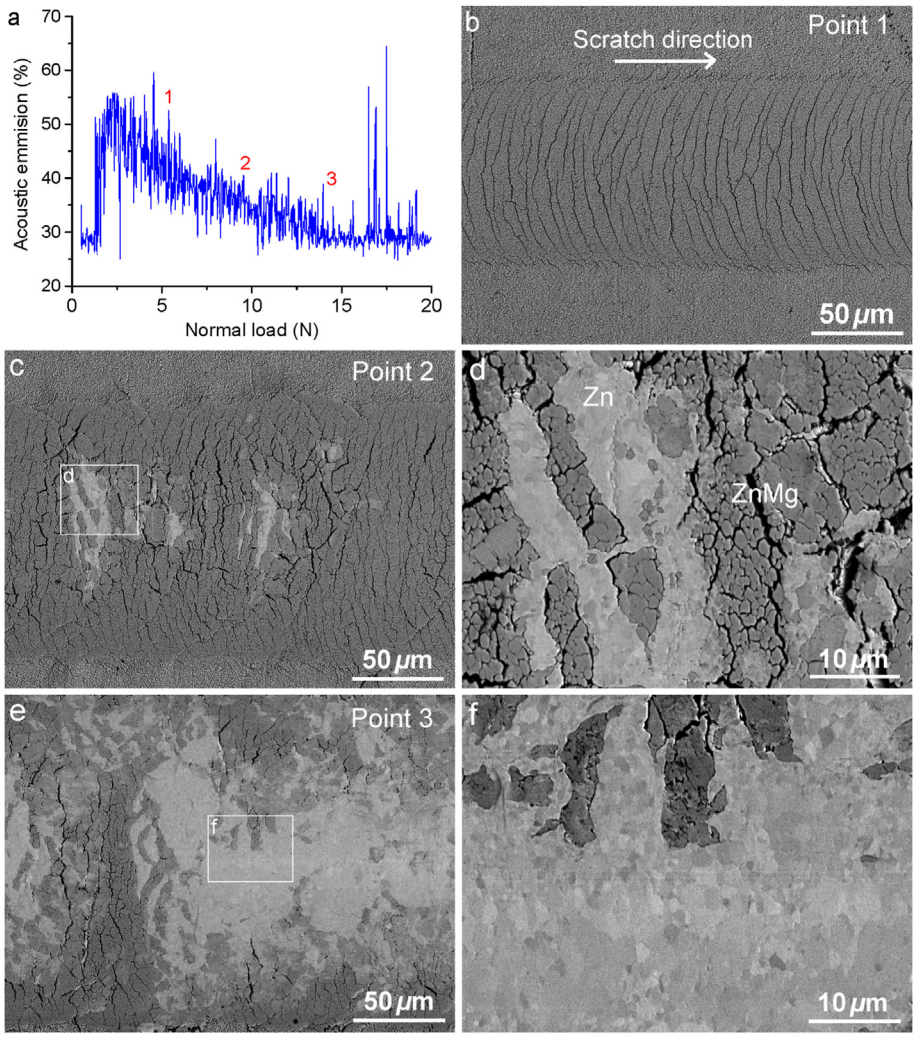


**Fig. 5.** (a) Acoustic emission curve versus normal load obtained for the as-deposited ZnMg11−Zn bilayer coating during the scratch test, SEM micrographs at different normal loads: (b) Point 1, (c, d) Point 2, and (d, e) Point 3.

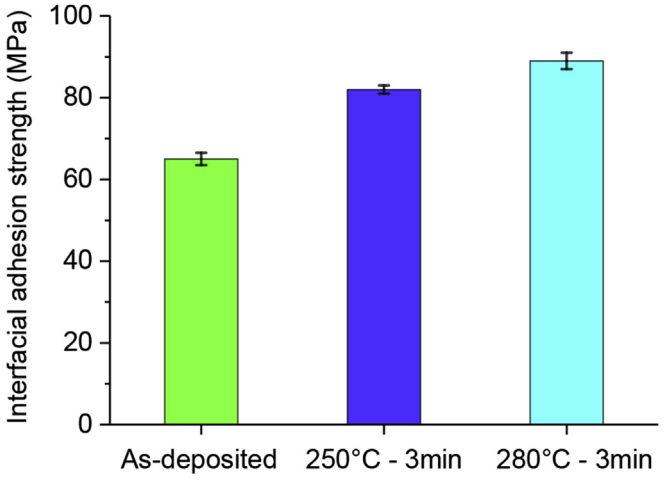


**Fig. 6.** Interfacial adhesion strength of the as-deposited and annealed ZnMg11−Zn coatings.

Considering the importance of the adhesion in sheet forming process, scratch test was used to measure the interfacial adhesion strength of the coatings, in as-deposited and annealed conditions. A typical acoustic emission curve versus normal load obtained during the scratch test of the as-deposited coating is shown in Fig. 5a. Through thickness Hertzian cracks were found along the scratch groove when the applied normal load is lower than the critical load $L_c$ (Fig. 5b). The ZnMg top layer starts to delaminate from the interface of ZnMg/Zn at the critical load of ~8.9 N, possibly due to the buckling phenomena. The Zn interlayer is clearly visible ahead of each buckled region (Fig. 5c–d). Progressive delamination of ZnMg is observed with increasing the normal load, where the large parts of the ZnMg top layer is delaminated from the Zn interlayer at the normal load of 14 N (Fig. 5e–f). With the same approach, the critical load of delamination is measured as 11.6 N and 12.5 N for the coating annealed for 3 min at 250 °C and 280 °C, respectively. The modified Benjamin-Weaver model was then used to calculate the adhesion strength of the coatings from the data obtained by the scratch test. The as-deposited coating exhibits the adhesion strength of 65 MPa. It increases to 82 and 88 MPa after 3 min of annealing at 250 and 280 °C, respectively (Fig. 6). This corresponds to at least 25 % increase in the interfacial adhesion strength. Both the coatings annealed at 250 and 280 °C for 3 min pass the BMW adhesion test. However, the annealed coatings fail the BMW adhesion test when the thickness of Zn intermediate layer is reduced to less than the critical thickness (as seen in Fig. 3d) or after

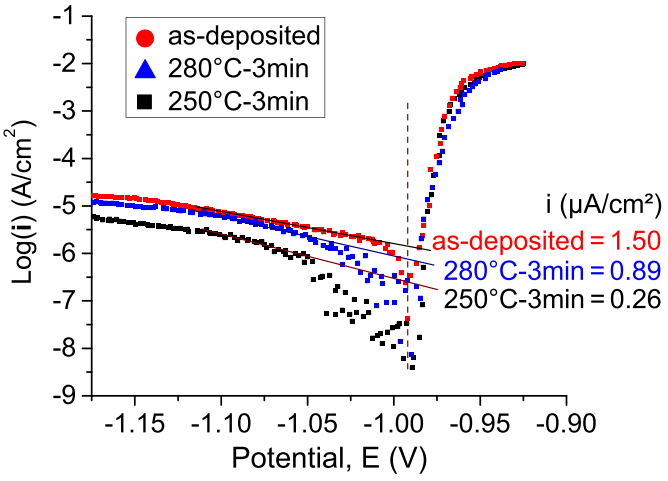


**Fig. 7.** Typical E-log(i) curve of the as-deposited and annealed ZnMg11−Zn coatings.

the complete dissolution of pure Zn and the subsequent formation of thick Fe−Zn intermetallic (as observed in Fig. 4d−f). The Fe−Zn intermetallic with a brittle structure is not able to accommodate the shear deformation and therefore, its formation should be avoided during annealing treatments.

### 3.3. Corrosion characterization

Tafel polarization tests were performed on the as-deposited and annealed samples (250°C-3min and 280°C-3min) to understand the correlation between the microstructure variations and the corrosion performance. The average roughness of the as-deposited coating (52 ± 3 nm) remains almost constant after annealing of 3 min at 250 °C and 280 °C (see Table 1). In this case, it means that the surface roughness does not play a role in the corrosion behavior of the tested samples. It is worth mentioning that the outmost surface of the 3 min annealed sample at 250 °C is composed of $MgZn_2$ while it is covered with $Mg_2Zn_{11}$ after the annealing treatment at 280 °C. Fig. 7 shows the typical examples of E-Log (i) curves for the as-deposited and annealed coatings. All of the coatings show closely similar corrosion potential; however the annealed coatings show better corrosion resistance compared to the as-deposited coating. The average corrosion current density of the coatings annealed at 250 °C and 280 °C is decreased to 0.52 ± 0.23 and 0.75 ± 0.15 μA/cm$^2$, respectively, compared to the as-deposited condition (0.91 ± 0.43 μA/cm$^2$). Improved corrosion performance of the annealed coating at 250 °C for 3 min can be explained by the formation of $MgZn_2$ intermetallic phase, containing higher Mg content at the surface after annealing. As Mg is pretty reactive, in principle it is expected that the relatively high-Mg content intermetallics should be more reactive. However, it has been proposed that the anodically susceptible intermetallic phase causes the initial formation of magnesium hydroxide corrosion product that deposits on the surface as a protective layer [20]. Meanwhile, the process in turn moderates the pH at local Zn-rich regions, inducing a compacted and protective simonkolleite layer against corrosion. With high Mg content, the process on coating surface is more efficient and the increase in resistance is faster. In addition, the annealed coating at 250 °C for 3 min is composed of a dense and compact outmost surface layer of $MgZn_2$ intermetallic (Fig. 4a and b), which is more uniform than that of the as-deposited samples (a mixture of $MgZn_2$ and $Mg_2Zn_{11}$ as seen in Fig. 2b), leading to more uniform protections [21].

## 4. Conclusions

In the present study, diffusion of the Zn and Mg elements across the interface of ZnMg/Zn was modeled for the heat treatment of PVD deposited ZnMg−Zn bi-layer coating in order to predict possible phase transformations during the annealing treatment. The results of the simulation are in good agreement with the experimental observations. Phase transformations initiate with the formation of a thin layer of $Mg_2Zn_{11}$ at the lower part of the top layer and a two-phase mixture of $Mg_2Zn_{11}$ and $MgZn_2$ phases at the upper part. At the intermediate stages of the annealing, $Mg_2Zn_{11}$ is the dominant phase in the top layer while the pure Zn in the intermediate layer is continuously consumed. Further annealing results in a complete dissolution of the pure Zn, formation and growth of a thick Fe−Zn intermetallic and reverse transformation of $Mg_2Zn_{11}$ to $MgZn_2$. The “high temperature fast annealing” can be designed accordingly to tailor the microstructure of the ZnMg−Zn coatings and achieve improved interfacial adhesion strength and anti-corrosion performance.

## Declaration of competing interest

The authors declare that they have no known competing financial interests or personal relationships that could have appeared to influence the work reported in this paper.

## CRediT authorship contribution statement

**S. Sabooni:** Conceptualization, Data curation, Investigation, Methodology, Formal analysis, Writing - original draft. **E. Galinmoghaddam:** Data curation, Investigation, Writing - original draft. **A.A. Turkin:** Software, Validation, Formal analysis, Writing - original draft. **L.Q. Lu:** Data curation, Investigation, Formal analysis. **R.J. Westerwaal:** Investigation, Data curation, Writing - review & editing. **C. Boelsma:** Writing - review & editing. **E. Zoestbergen:** Writing - review & editing. **Y.T. Pei:** Funding acquisition, Conceptualization, Methodology, Formal analysis, Writing - review & editing, Supervision.

## Acknowledgment

This research was carried out under project number S22.3.13513a in the framework of the Partnership Program of the Materials innovation institute M2i (www.m2i.nl) and the Technology Foundation TTW (www.stw.nl), which is part of the Netherlands Organization for Scientific Research (NWO, www.nwo.nl). The Netherlands Organization for Scientific Research is acknowledged for awarding to A.A.T the visitor grant 040.11.688.

## References

[1] J. Mackowiak, N.R. Short, Metallurgy of galvanized coatings, Int. Met. Rev. 24 (1979) 1−19.
[2] M. Dutta, A.K. Halder, ShB. Singh, Morphology and properties of hot dip Zn-Mg and Zn-Mg-Al alloy coatings on steel sheet, Surf. Coating. Technol. 205 (2010) 2578−2584.
[3] C. Yao, Z. Wang, S.L. Tay, T. Zhu, W. Gao, Effects of Mg on microstructure and corrosion properties of Zn−Mg alloy, J. Alloys Compd. 602 (2014) 101−107.
[4] J.H. La, M.G. Song, H.K. Kim, S.Y. Lee, W.S. Jung, Effect of deposition temperature on microstructure, corrosion behavior and adhesion strength of Zn-Mg coatings on mild steel, J. Alloys Compd. 739 (2018) 1097−1103.
[5] C. Yao, H. Lv, T. Zhu, W. Zheng, X. Yuan, W. Gao, Effect of Mg content on microstructure and corrosion behavior of hot dipped Zn-Al-Mg coatings, J. Alloys Compd. 670 (2016) 239−248.
[6] P. Volovitch, T.N. Vu, C. Allély, A. Abdel Aal, K. Ogle, Understanding corrosion via corrosion product characterization: II. Role of alloying elements in improving the corrosion resistance of Zn-Al-Mg coatings on steel, Corrosion Sci. 53 (2011) 2437−2445.
[7] S. Sabooni, E. Galinmoghaddam, M. Ahmadi, R.J. Westerwaal, J. van de

Langkruis, E. Zoestbergen, J.ThM. De Hosson, Y.T. Pei, Microstructure and adhesion strength quantification of PVD bi-layered ZnMg-Zn coatings on DP800 steel, Surf. Coating. Technol. 359 (2019) 227–238.
[8] A.C. Karaoglanli, H. Dikici, Y. Kucuk, Effects of heat treatment on adhesion strength of thermal barrier coating systems, Eng. Fail. Anal. 32 (2013) 16–22.
[9] J.M. Byun, S.Y. Bang, H.W. Kim, T.Y. Kim, S.J. Hong, Y.D. Kim, Effect of heat treatment on corrosion resistance and adhesion property in Zn-Mg-Zn multi-layer coated steel prepared by PVD process, Surf. Coating. Technol. 309 (2017) 1010–1014.
[10] E. Zoestbergen, J. van de Langkruis, T.F.J. Maalman, E. Batyrev, Influence of diffusion on the coating adhesion of zinc-magnesium thin films onto steel, Surf. Coating. Technol. 309 (2017) 904–910.
[11] S. Sabooni, E. Galinmoghaddam, H.T. Cao, R.J. Westerwaal, E. Zoestbergen, J.ThM. De Hosson, Y.T. Pei, New insight into the loss of adhesion of ZnMg-Zn bi-layered coatings, Surf. Coating. Technol. 370 (2019) 35–43.
[12] D. Gimenez-Romero, J.J. Garcia-Jareno, F. Vicente, Correlation between the fractal dimension of the electrode surface and the EIS of the zinc anodic dissolution for different kinds of galvanized steel, Electrochem. Commun. 6 (2004) 148–152.
[13] T.C. Illingworth, I.O. Golosnoy, Numerical solutions of diffusion-controlled moving boundary problems which conserve solute, J. Comp. Physiol. 209 (2005) 207–225.
[14] M. Mezbahul-Islam, A.O. Mostafa, M. Medraj, Essential magnesium alloys binary phase diagrams and their thermochemical data, J. Mater. (2014) 1–33. Article ID 704283.
[15] P. Ghosh, M. Mezbahul-Islam, M. Medraj, Critical assessment and thermodynamic modeling of Mg–Zn, Mg–Sn, Sn–Zn and Mg–Sn–Zn systems, Calphad 36 (2012) 28–43.
[16] A. Mostafa, M. Medraja, On the atomic interdiffusion in Mg-{Ce, Nd, Zn} and Zn-{Ce, Nd} binary systems, J. Mater. Res. 29 (2014) 1463–1479.
[17] S.K. Das, Y.M. Kim, T.W. Ha, I.H. Jung, Investigation of an isotropic diffusion behavior of Zn in hcp Mg and interdiffusion coefficients of intermediate phases in the Mg-Zn system, Calphad 42 (2013) 51–58.
[18] R. Filipek, K. Szyszkiewicz, P. Dziembaj, P. Skrzyniarz, A. Wierzbicka-Miernik, P. Zieba, Modeling of reactive diffusion: mechanism and kinetics of the intermetallics growth in Ag/Ag interconnections, J. Mater. Eng. Perform. 21 (2013) 638–647.
[19] S. Sabooni, M. Ahmadi, E. Galinmoghaddam, R.J. Westerwaal, C. Boelsma, E. Zoestbergen, G.M. Song, Y.T. Pei, Fundamentals of the adhesion of physical vapor deposited ZnMg-Zn bilayer coatings to steel substrates, Mater. Des. 190 (2020) 108560.
[20] N.C. Hosking, M.A. Ström, P.H. Shipway, C.D. Rudd, Corrosion resistance of zinc–magnesium coated steel, Corrosion Sci. 49 (2007) 3669–3695.
[21] R. Krieg, A. Vimalanandan, M. Rohwerder, Corrosion of zinc and Zn-Mg alloys with varying microstructures and magnesium contents, J. Electrochem. Soc. 161 (2014) C156–C161.